



LAWRENCE
LIVERMORE
NATIONAL
LABORATORY

Characterization of Shock Waves in Solids Using a Fiber Optic Pressure Probe

G. A. Cranch, R. Lunsford, J. Grun, J. Weaver, S.
Compton, M. May, N. Kostinski

April 17, 2013

Applied Optics

Disclaimer

This document was prepared as an account of work sponsored by an agency of the United States government. Neither the United States government nor Lawrence Livermore National Security, LLC, nor any of their employees makes any warranty, expressed or implied, or assumes any legal liability or responsibility for the accuracy, completeness, or usefulness of any information, apparatus, product, or process disclosed, or represents that its use would not infringe privately owned rights. Reference herein to any specific commercial product, process, or service by trade name, trademark, manufacturer, or otherwise does not necessarily constitute or imply its endorsement, recommendation, or favoring by the United States government or Lawrence Livermore National Security, LLC. The views and opinions of authors expressed herein do not necessarily state or reflect those of the United States government or Lawrence Livermore National Security, LLC, and shall not be used for advertising or product endorsement purposes.

Characterization of Shock Waves in Solids Using a Fiber Optic Pressure Probe

Geoffrey A. Cranch,¹ Robert Lunsford,¹ Jacob Grün,¹ James Weaver,¹ Steve Compton,² Mark May,² and Natalie Kostinski²

¹*Naval Research Laboratory, Code 5674, 4555 Overlook Avenue SW, Washington, DC 20375*

²*Lawrence Livermore National Laboratory, 7000 East Ave B663-L72, Livermore, CA 94550*

compiled: March 25, 2013

Measurement of shock wave pressure in solid blocks of polymethyl methacrylate is demonstrated using fiber optic pressure probes. Three probes based on a fiber Fabry-Perot, fiber Bragg grating and interferometric fiber tip sensor are tested and compared. Shock waves are generated using a high power laser focused onto a thin foil target placed in close proximity to the test blocks. The fiber Fabry-Perot sensor appears capable of resolving the shock front with a rise time of 91 ns. The peak pressure is estimated using a separate shadowgraphy measurement to be 3.4 GPa.

OCIS codes: 000.0000, 999.9999.

1. Introduction

Direct measurements on shock waves propagating in solid media are difficult due to the high pressure generated by the shock. In transparent media, optical imaging techniques can be used to image the shock front, from which shock wave speed and peak pressure can be determined. However, in opaque media, measurement techniques are limited. A pressure sensor must be sufficiently rigid to withstand the shock wave, which may generate pressures around 10^{10} Pa. It must also be sufficiently small to provide a fast response time and to avoid measurement error due to the curvature of the shock front. Events that generate shock waves also generate large amounts of electromagnetic energy, which can interfere with electronic sensors.

Dielectric sensors, such as those based on fiber optics, can provide immunity from electromagnetic interference, a sufficiently small sensor head capable of a fast response time and a solid sensor head capable of withstanding extremely high pressures in a solid structure. Such a measurement capability will enable improved understanding of shock wave propagation in solid media by determining material characteristics such as shock wave speed and its relationship to shock pressure as well as behavior of the shock wave at interfaces and boundaries.

There have been many reported demonstrations of fiber optic sensors for measurement of ultrasonics and shock waves in liquids and air. The fiber Bragg grating (FBG) strain sensor has been investigated for measurement of ultrasonics in water [1–3]. Fabry-Perot sensors based on an air-backed diaphragm formed on the tip of an optical fiber have been reported for measurement of blast driven shock waves in air [4–7]. A solid Fabry-Perot formed on the tip of a fiber has also been reported

for measurement of ultrasonics in liquids [8]. A fiber tip sensor based on measurement in the change in the Fresnel reflection at the fiber endface has been demonstrated [9]. This utilizes the dependence of the refractive index on pressure in water, which modulates the reflected intensity from the fiber endface. This technique has been improved by using a tapered gold coated fiber tip [10]. Another fiber tip sensor based on the measurement of the phase shift in the light reflected from a mirrored fiber end, that forms one arm of a Michelson interferometer, has also been demonstrated for measurements of shock waves in liquids [11, 12].

Despite numerous demonstrations of shock wave measurement in air and liquids, there have been no demonstrations in solids using fiber optic pressure sensors. In the current work, three types of fiber optic pressure sensor have been integrated into polymethyl methacrylate (PMMA) test blocks. Shock waves are generated by focusing the output of a multi-beam Kr:F laser onto a target attached to the test block. The target consists of a metal or plastic foil. The tests have been carried out in a high energy laser facility known as the NIKE facility [13, 14]. This facility generates a pulse energy up to 2 kJ with a total of 48 beams and a pulse duration of 4 ns at 248 nm. For these tests, the pressure sensor must be capable of withstanding pressures up to 10 GPa with a rise time less than 100 ns.

The fiber optic pressure sensors under test are formed on the tip of an optical fiber and are based on a solid fiber Fabry-Perot [8], a fiber Bragg grating and a fiber tip interferometric sensor [11]. Preliminary tests provide a direct comparison of the response of these sensors. Further tests carried out on Fabry-Perot type sensors provide an indication of measurement consistency and

repeatability. The use of a transparent PMMA block also enables simultaneous imaging of the shock wave using shadowgraphy[15]. Estimates of the shock wave speed from the shadowgraphy measurements enable a basic pressure calibration of the sensor to be performed.

The manuscript is arranged as follows. The next section describes the operating principle of the three types of pressure sensor and the shadowgraphy measurement. Section 3 describes the facility used to conduct the laser generated shock experiments, experimental procedure and the results from the pressure measurements for the three probes and the shadowgraphy measurement. Finally, key results are summarized in section 4.

2. Shock wave measurement techniques

2.A. Pressure sensors

The basic principle of the fiber tip sensor is shown in fig. 1. A shock wave entering the fiber from the right causes a change in optical path length (OPL) of the optical fiber. This OPL change arises from both a change in physical length of the fiber and a change in refractive index. This change in path length can be measured by placing an optical device at the tip of the fiber that can respond to this length change.

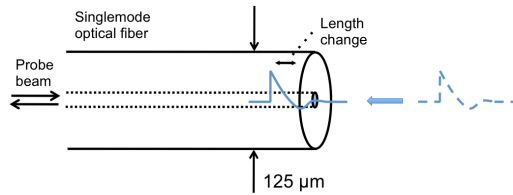


Fig. 1. Operating principle of fiber optic pressure probe

Three sensor types have been employed to measure this change in OPL. These are now described.

2.A.1. Fiber Fabry-Perot sensor

The fiber Fabry-Perot sensor is of the type described in [8]. It consists of a two gold coating mirrors separated by a $10 \mu\text{m}$ thick polymer spacer (Parylene-C), as illustrated in the inset of fig. 2(a). This is formed on the tip of a single mode optical fiber, which is $125 \mu\text{m}$ in diameter. A single frequency laser (HP81689A) is tuned to the lower wavelength half-power point of the optical resonance as illustrated in fig. 3(a). A change in the thickness of the polymer spacer due to the shock wave will change the position of the resonance, causing a change in the reflected intensity of the laser. If this change is small compared to the spectral width of the resonance, the change in intensity will scale linearly with the change in resonance position. The received power is detected with a high bandwidth photodiode receiver (TTI TIA-500). The received power was -11 dBm.

2.A.2. Fiber Bragg grating sensor

A fiber Bragg grating is inscribed in a single mode optical fiber(SMF-28) using a phase mask at 244 nm (CW). This fiber was cleaved to form a $0.5 \text{ mm} \pm 100 \mu\text{m}$ long

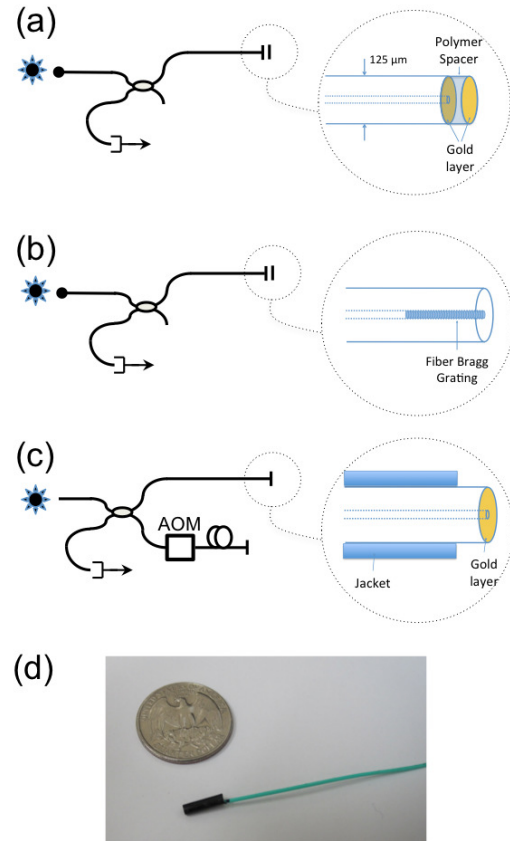


Fig. 2. Pressure sensors: (a) fiber Fabry-Perot, (b) fiber Bragg grating, (c) Michelson interferometer, and (d) packaged sensor.

FBG at the tip of the fiber (an angle cleave was used to reduce the Fresnel reflection from the fiber end), as shown in the inset of fig. 2(b). The FBG length was monitored using an optical frequency domain reflectometer.

The FBG sensor, shown in fig. 2(b), was interrogated by tuning a single frequency laser (HP81689A) to the half-power point of the reflection spectrum, as illustrated in fig. 3(b), and measuring the intensity of the reflected laser signal on a photodiode receiver (TTI TIA-500). The peak power reflectivity of the FBG was approximately 1 % and yielded a received power of -20 dBm.

2.A.3. Michelson interferometer fiber tip sensor

The Michelson interferometer (MI) based sensor comprises a cleaved optical fiber with a mirror coating formed on the end face. This fiber is placed in one arm of a fiber optic Michelson interferometer. The other arm contains an acousto-optic modulator (AOM) and a second mirrored fiber end. The interferometer is probed with a coherent laser (NP Photonics), such that a heterodyne carrier at 200 MHz is generated at the detector (New Focus 1554). Shock induced length changes in the fiber tip will modulate the phase of the heterodyne fre-

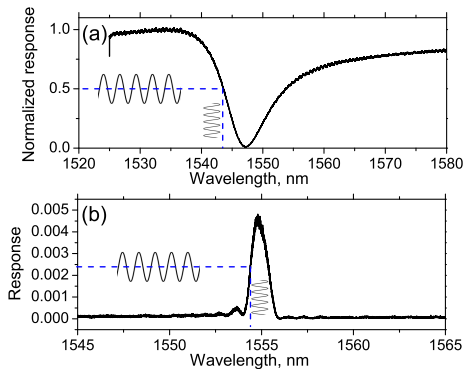


Fig. 3. Optical spectra of: (a) fiber Fabry-Perot and (b) fiber Bragg grating. These are measured by scanning a tunable laser across the resonance and recording the reflected power.

quency. The carrier is downconverted to 20 MHz and recorded as a time series on a digital oscilloscope. The phase information is extracted using a Hilbert Transform to determine the instantaneous frequency. Temporal integration of this signal provides the required phase information.

Before insertion into the PMMA block, these sensors are molded into a cylinder of high thermal heat transfer epoxy (50-3100) measuring 3 mm diameter by 6 mm long, shown in fig. 2(d). The tip of the sensor is aligned with the end face of the cylinder and the fiber exits the other end of the cylinder through a bifurcation tube.

The fiber Fabry-Perot and fiber Bragg grating sensors provide a point-like measurement of the local displacement. Displacements occurring outside of the Fabry-Perot or FBG do not contribute to the response. However, the interferometer responds to displacements anywhere along the sensing fiber. To ensure adequate response time is obtained, the shock wave must not propagate far along the fiber. Only the fiber tip is adhered to the epoxy to reduce the propagation of the shock wave along the fiber. The trailing fiber is loosely contained with the bifurcation tube. This sensor has a number of benefits over the Fabry-Perot and FBG sensors. By encoding the displacement information as a phase modulation, the dynamic range of the sensor is determined by the available bandwidth, which is set by the carrier frequency. A larger dynamic range is obtained by increasing the carrier frequency without any loss of linearity or sensitivity. Interferometric measurement is also expected to yield a higher sensitivity.

2.B. Shadowgraphy

The shock wave is also imaged as it propagates through the test block using shadowgraphy [15]. The block is illuminated with a Verdi V-10 diode-pumped laser (Coherent Inc). The beam is expanded, collimated and passed through the side of the test block before being imaged onto a high speed SIM 8 camera (Photo-Sonics

Inc). The camera aperture is open for 50 ns and the frame rate 3 μ s.

3. Experimental Procedure and Results

Initial tests were carried out on a PMMA block incorporating all three sensors. The sensors were placed in parallel approximately 30 mm from the target face, as shown in the upper left of fig. 4. For these tests, the NIKE laser operated with 40 beams at 34.6 J/beam giving a total pulse energy of 1.38 kJ at 248 nm. This was focused in a 1 mm spot size onto a foil target mounted onto the front face of the test block. This block was placed in a vacuum chamber, illustrated in fig. 4. The sensor fibers exit the vacuum chamber through a custom designed fiber optic feed-through. This is connected to the optoelectronic units through a 25 m cable, contained within a separate shielded room. Data are recorded on a digital oscilloscope that is triggered by an appropriately delayed signal from the laser facility. The results from a shot on this block are shown in fig. 5.

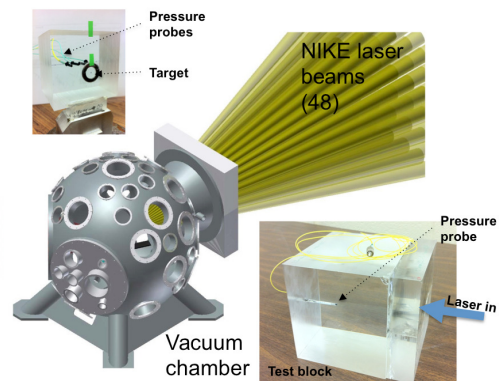


Fig. 4. General schematic of laser induced shock system (upper left) three pressure probes installed in test block for initial tests and (lower right) Fabry-Perot sensor installed in test block

The Fabry-Perot sensor captures the shock front that arrives at 11.5 μ sec. The increase in pressure due to the shock wave compresses the sensor tip, causing the resonance to shift to shorter wavelength. This produces a reduction in the reflected power and therefore a drop in the measured voltage. The sensor output voltage is observed to increase after this initial drop and then decrease again. This behavior occurs due to the resonance minimum, shown in fig. 3(a), being shifted to a lower wavelength than the probe wavelength (i.e. the sensor is driven beyond its linear region). The sensor is therefore capable of responding to the peak pressure produced by the shock, but must be linearized to obtain the correct response.

The fiber Bragg grating also responds to the shock, however significant oscillation is observed after the initial shock front has arrived and continues for the remainder of the signal. It will be shown later that the shock wave speed is approximately 3.7 km/s. Taking the rise

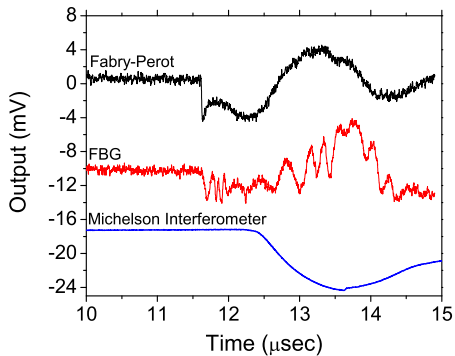


Fig. 5. Comparison of shock wave measurements for the fiber Fabry-Perot, fiber Bragg grating and Michelson interferometer. The oscillatory behavior observed in the FBG response arises from distortion of the FBG spectra due to the shock front.

time of the shock front from the Fabry-Perot measurement to be ~ 100 ns, this yields a spatial extent of ~ 0.4 mm, which is comparable to the length of the FBG. This nonuniform stress distribution across the FBG is likely to induce significant distortion of the FBG spectra, causing the oscillatory response observed in fig. 5.

The Michelson interferometer produces a smoothed and delayed response indicating that the bandwidth of the sensor response is much less than the other two sensors and not capable of resolving the shock front. It was determined that a large total path imbalance (~ 100 m) was present in the Michelson interferometer due to the long connecting lead to the vacuum chamber. This path imbalance causes the interferometer to behave as a low pass filter with a normalized frequency response given by $\hat{R} = |\sin(nL\omega_s/c)| / (nL\omega_s/c)$ where n is the fiber effective refractive index, L is the total fiber path imbalance, ω_s is the signal angular frequency, and c is the vacuum light velocity. Thus for $L = 100$ m and $\omega_s = 1$ MHz yields $\hat{R} \simeq 0.02$. High frequency signals are thus greatly attenuated. The large imbalance also makes deconvolving the interferometer response from the measured signal difficult, thus the true response time of the MI cannot be determined from this measurement and will be analyzed in future measurements. However, the signal to noise from the MI can be seen to be significantly better than the other two sensors, indicating that it provides a more sensitive measurement (the filtering effect of the imbalanced interferometer does not affect the noise generated on the detector and only acts to attenuate the measured signal).

Further tests were carried out on the Fabry-Perot sensor using a different test block, illustrated in the lower right of fig. 4. A target consisted of a foil placed inside a conic opening on one side of the PMMA block (labeled 'laser in'). A 1 mm air gap exists between the target and the PMMA block. The focused laser beam

impacts the target, which generates a shock wave propagating through the block. The tip of the pressure sensor is located 88.9 mm from the surface where the shock wave initiates. For these tests, the NIKE laser operated with 48 beams at 34.6 J/beam producing a total pulse energy of 1.66 kJ. The results from three separate shots are shown in fig. 6 (note that the later arrival time of the shot labeled 17may12_5 is due to a difference in trigger time of the digital oscilloscope).

For each shot, the response of the Fabry-Perot is driven beyond its region of linearity. To enable comparison, the three measurements were linearized by applying the response function, shown in fig. 3(a), to each dataset. The results are shown in fig. 7 and are plotted in terms of the shift of the optical resonance in wavelength. The measurement corresponding to 17may12_5 produced the smallest signal. However, it was later found that the target was mounted incorrectly in this test block and the block had exploded during testing. This may have reduced the efficiency with which the shock wave was generated within the block. The peak response measured for shot 22may12.1 was 28 % higher than for shot 22may12.2 and may be due to variation in the sensor response and/or error in the linearization procedure. Further tests are planned to establish the accuracy of the pressure measurement.

Fig. 8 shows a magnified view of the measurement corresponding to 22may12.2. The inset shows the rise time to be 91 ns for the initial shock front.

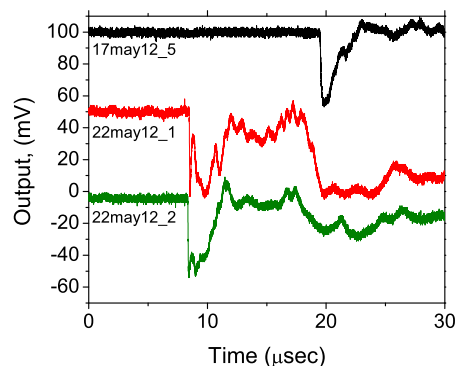


Fig. 6. Pressure measurements for three shots with the fiber Fabry-Perot

The results from a shadowgraphy measurement for the shot 22may12.1 are shown in fig. 9. Each frame corresponds to a temporal evolution of $3 \mu\text{s}$. The shock front, highlighted with an arrow in frame 1, reaches the sensor at frame 6. As it propagate past the probe in frames 7 and 8, the shock front is obscured by the opaque epoxy used to embed the pressure sensor. The velocity of the shock front is estimated from this measurement and the measurement for 22may12.2 to be 3.74 km/s in both cases, which is much higher than the linear sound ve-

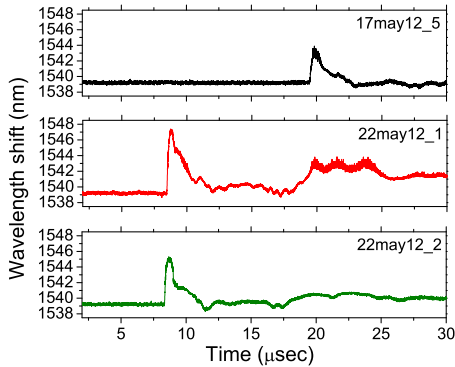


Fig. 7. Linearized measurements for three shots shown in fig. 6

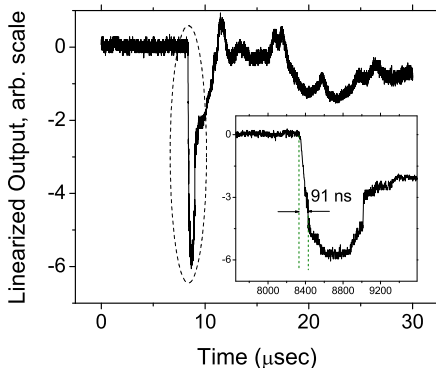


Fig. 8. Linearized pressure measurements from Fabry-Perot (22may12.2) (inset) shows an enlargement of the measured shock front. The horizontal scale is in nsec.

locity of ~ 2.75 km/s at 10 MHz and 25 °C[16]. Using published data for the relationship between the sound speed and shock wave pressure for PMMA [17–20], the peak pressure is estimated to be 3.4 GPa.

4. Conclusions

Three fiber optic pressure probes based on a fiber Fabry-Perot, fiber Bragg grating and interferometric fiber tip sensor have been used to characterize the pressure of laser generated shock waves in solid PMMA test blocks. The fiber Bragg grating and interferometric sensor had insufficient response speed (or bandwidth) to resolve the shock front, which was found to last 91 ns, making them unsuitable for determining the peak shock pressure. However, the bandwidth of the interferometric sensor was limited by a large imbalance in the interferometer and can be dramatically increased by path matching the interferometer. Further tests are required to establish the true response time of the interferometric sensor.

The fiber Fabry-Perot appears capable of resolving the shock front. The peak pressure exceeded the linear range of the Fabry-Perot sensor, however, the output could be linearized using the sensor response function. To avoid the need for linearization, the response to pressure of the Fabry-Perot sensor can be reduced by reducing the thickness of the polymer spacing separating the mirrors. Two measurements on test blocks incorporating Fabry-Perot pressure sensors showed a difference in peak response of 28 %. Simultaneous measurements of the shock speed and pressure using shadowgraphy show the peak shock pressure to be equal for both measurements. Therefore, further tests are planned to establish repeatability and accuracy of the pressure measurement. Simultaneous measurements of the shock wave propagation through the PMMA block using shadowgraphy enabled estimation of the shock wave speed to be 3.74 km/s with a peak pressure of 3.4 GPa.

All three sensors could withstand the shocks from multiple shots on the same test block.

5. Acknowledgments

This work is sponsored by the Defense Threat Reduction Agency and performed under the auspices of the U.S. Department of Energy by Lawrence Livermore National Laboratory under Contract DE-AC52-07NA27344.

References

- [1] N. E. Fisher, D. J. Webb, C. N. Pannell, D. A. Jackson, L. R. Gavrilov, J. W. Hand, L. Zhang, and I. Bennion, *Applied Optics* **37**, 8120 (1998).
- [2] P. Fomitchov and S. Krishnaswamy, *Optical Engineering* **42**, 956 (2003).
- [3] G. Flockhart, M. McGuire, S. Pierce, G. Thursby, G. Stewart, G. Hayward, and B. Culshaw, *Proceedings of SPIE - The International Society for Optical Engineering* **7503** (2009).
- [4] W. N. MacPherson, M. J. Gander, J. S. Barton, J. D. C. Jones, C. L. Owen, A. J. Watson, and R. M. Allen, *Measurement Science and Technology* **11**, 95 (2000).
- [5] S. Watson, M. J. Gander, W. N. MacPherson, J. S. Barton, J. D. C. Jones, T. Klotzbuecher, T. Braune, J. Ott, and F. Schmitz, *Applied Optics* **45**, 5590 (2006).
- [6] S. Watson, W. N. MacPherson, J. S. Barton, J. D. C. Jones, A. Tyas, A. V. Pichugin, A. Hindle, W. Parkes, C. Dunare, and T. Stevenson, *Measurement Science and Technology* **17**, 1337 (2006).
- [7] W. Parkes, V. Djakov, J. S. Barton, S. Watson, W. N. MacPherson, J. T. M. Stevenson, and C. C. Dunare, *Journal of Micromechanics and Microengineering* **17**, 1334 (2007).
- [8] P. Morris, A. Hurrell, A. Shaw, E. Zhang, and P. Beard, *Journal of the Acoustical Society of America* **125**, 3611 (2009).
- [9] J. Staudenraus and W. Eisenmenger, *Ultrasonics* **31**, 267 (1993).

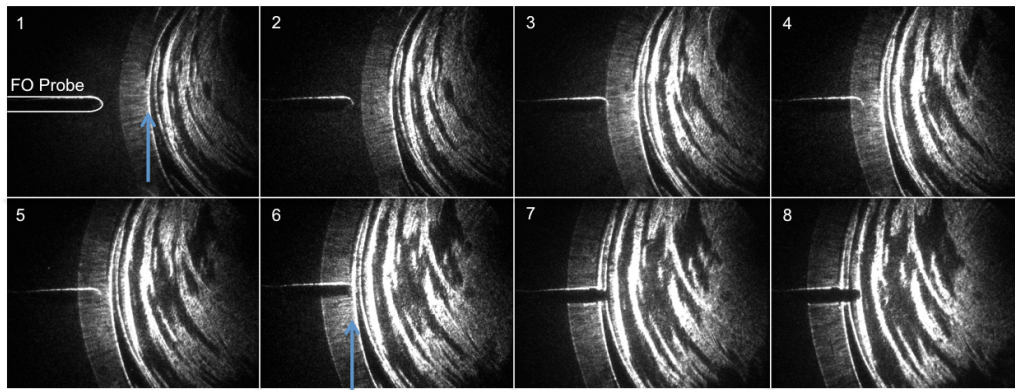


Fig. 9. Shadowgraphy measurement for shot 22may12_1.

- [10] R. G. Minasamudram, P. Arora, G. Gandhi, A. S. Daryoush, M. A. El-Sherif, and P. A. Lewin, *Applied Optics* **48**, G77 (2009).
- [11] C. Koch, G. Ludwig, and W. Molkenstruck, *Ultrasonics* **36**, 721 (1998).
- [12] C. Koch and K.-V. Jenderka, *Ultrasonics Sonochemistry* **15**, 502 (2008).
- [13] T. Lehecka, S. Bodner, A. V. Deniz, A. N. Mostovych, S. P. Obenschain, C. J. Pawley, and M. S. Pronko, *Journal of Fusion Energy* **10**, 301 (1991).
- [14] J. D. Sethian, M. Myers, J. L. Giuliani, R. Lehmborg, P. Kepple, M. F. Wolford, F. Hegeler, M. Friedman, S. B. Swanekamp, D. Weidenheimer, and D. Rose, in *Inertial Fusion Sciences and Applications 2003* (2004) pp. 517–522.
- [15] G. S. Settles, *Schlieren and shadowgraph techniques: Visualizing phenomena in transparent media* (Springer-Verlag, Berlin, 2001).
- [16] J. E. Carlson, in *IEEE Symposium on Ultrasonics* (2003) pp. 885–888.
- [17] D. Moore, D. Funk, and S. McGrane, *At the Confluence of Experiment and Simulation: Ultrafast Laser Spectroscopic Studies of Shock Compressed Energetic Materials in Chemistry at Extreme Conditions*, edited by M. Riad Manaa (Elsevier, Amsterdam, 2005).
- [18] L. Barker and R. E. Hollenbach, *J. Appl. Phys.* **41** (1970).
- [19] S. Marsh, *LASL Shock Hugoniot Data*. (University of California Press, Berkley, CA, 1980).
- [20] D. R. Christman, *Final Report to the Defense Nuclear Agency Report No. MSL-71-24 / DNA2810F* (1980).